Lessons from and best practices for the deployment of the Soil Water Isotope Storage System

Rachel E. Havranek [1], Kathryn Snell[1], Sebastian Kopf[1], Brett Davidheiser-Kroll[2], Valerie Morris[3], Bruce Vaughn[3]

Rachel Havranek, Kathryn Snell, Sebastian Kopf, Brett Davidheiser-Kroll, Valerie Morris, Bruce Vaughn

[1]Geological Sciences, University of Colorado Boulder, Boulder, 80303, USA

[2]Thermo Fisher Scientific (Bremen) GmbH, Bremen, Germany

[3]Institute of Arctic and Alpine Research, University of Colorado Boulder, Boulder, 80303, USA

Correspondence to: Rachel Havranek (rachel.havranek@colorado.edu)

Abstract. Soil water isotope datasets are useful for understanding connections between the hydrosphere, atmosphere, biosphere, and geosphere. However, they have been underproduced because of technical challenges associated with collecting those datasets. Here, we present the full testing and automation of the Soil Water Isotope Storage System (SWISS). The unique innovation of the SWISS is that we are able to automatically collect water vapor from the critical zone at a regular time interval and then store that water vapor until it can be measured back in a laboratory setting. Through a series of quality assurance and quality control tests, we rigorously tested that the SWISS is resistant to both atmospheric intrusion and leaking in both laboratory and field settings. We assessed the accuracy and precision of the SWISS through a series of experiments where water vapor of known composition was introduced into the flasks, stored for 14 days, and then measured. From these experiments, after applying an offset correction, we assess the precision of the SWISS at 0.9‰ and 3.7‰ for $\delta^{18}O$ and δ^2H, respectively. We deployed three SWISS units to three different field sites to demonstrate that the SWISS stores water vapor reliably enough that we are able to differentiate dynamics both between the sites as well within a single soil column. Overall, we demonstrate that the SWISS is able to faithfully retain the stable isotope composition of soil water vapor for long enough to allow researchers to address a wide range of ecohydrologic questions.

1 Introduction

Understanding soil water dynamics across a range of environments and soil properties is critical to food and water security (e.g. Mahindawansha et al., 2018; Quade et al., 2019; Rothfuss et al., 2021); understanding biogeochemical cycles, such as the the nitrogen and phosphorus cycles (e.g. Hinckley et al., 2014; Harms and Ludwig, 2016); and understanding connections between the hydrosphere, biosphere, geosphere and atmosphere (e.g. Vereeken et al., 2022). One approach that can be used to understand water use and movement in the critical zone is the stable isotope geochemistry of soil water (e.g. Sprenger et al., 2016; Bowen et al., 2019). Variations in the stable isotope ratios of oxygen and hydrogen of soil water ($\delta^{18}O$, δ^2H) track physical processes like infiltration, root uptake

32   and evaporation. In particular, stable water isotopes are useful for disentangling complex mixtures of water from

33   multiple sources (e.g. Dawson and Ehleringer, 1991; Brooks et al., 2010; Soderberg et al., 2012; Good et al., 2015;

34   Bowen et al., 2018; Gomez-Navarro et al., 2019; Sprenger and Allen 2020). Despite the long-recognized utility of

35   measuring soil water isotopes for understanding a range of processes (e.g. Zimmerman et al., 1966; Peterson & Fry.,

36   1987), soil water isotope datasets have been under-produced as compared to groundwater and meteoric water

37   isotope datasets (Bowen et al., 2019).

38   The primary barrier to producing soil water isotope datasets has been the arduous nature of collecting

39   samples. Traditionally, soil water samples are taken by digging a pit, and collecting a mass of soil to bring back to

40   the lab for subsequent water extraction, disrupting the soil profile each time a sample is collected. To circumvent

41   issues related to this style of sampling, the ecohydrology community has developed a variety of in situ water

42   sampling methods over the last 10 years (e.g. Rothfuss et al., 2013; Volkmann and Weiler, 2014; Gaj et al., 2015;

43   Oerter et al., 2016; Beyer et al., 2020). These methods have helped to shed light on a range of ecohydrologic

44   questions from evaporation and water use dynamics in managed soils (e.g. Oerter et al., 2017; Quade et al., 2019) to

45   better understanding where plants and trees source their water (e.g. Beyer et al., 2020).

46   The expansion in situ sampling methods allows for a greater understanding of ecohydrologic dynamics

47   temporally, but with current methods these studies are often done in close proximity to the institutions performing

48   the studies because of logistical constraints. The spatial constraints limit what we can learn about soil hydrology in

49   remote and traditionally understudied landscapes. Beyond the ecohydrology community, the creation of high

50   temporal resolution soil water isotope data sets is useful to a broader set of stakeholders. For example, long-term

51   temporal records of soil water can be used to better understand geologic proxy development (e.g. stable isotope

52   records from pedogenic carbonate, br-GDGTs, etc.). These projects, however, commonly have environmental

53   constraints like soil type or local climate state that may not be located near institutions performing those studies,

54   creating the need for a system that is capable of collecting water vapor from remote settings in an automated way.

55   In this contribution, we report on the further development and testing of a field deployable system first

56   introduced in Havranek et al., (2020). This system is now capable of independently sampling soil water vapor in

57   situ, storing that water vapor for a period of time until the samples can be brought back to a laboratory to be

58   measured. In our case, we used a Picarro L-2130*i* water isotope analyzer (Picarro, Inc. Santa Clara, CA) to measure

59   both water concentration and the oxygen and hydrogen isotope ratios of the soil water vapor. The combination of the

60   autonomous sampler and the CRDS instrument offers a flexible and reliable solution to obtain data that is otherwise

61   difficult to collect from soil profiles. Here, we present the testing and optimization of the Soil Water Isotope Storage

62   System (SWISS). First, we present a quality assurance and quality control (QA/QC) procedure that we strongly

63   recommend any future user to complete prior to deploying this kind of system for either a field or lab experiment.

64   Second, we demonstrate the viability of this system under field-conditions through two field suitability experiments.

65   Lastly, we sampled three different field sites to show that the automation schema works on a monthly timescale and

66   that the system preserves soil water vapor isotopes signals with sufficient precision to distinguish between three

67   different field settings and vertical profile differences.

2 Background

In recent years, a number of technical innovations have made it easier to sample and measure soil water for stable isotope analysis. Advances in laser-based instrumentation (e.g. cavity ring-down spectroscopy, CRDS) have made high throughput, high precision measurements of both water concentration and water stable isotopes possible. Field deployments with laser-based instruments are technically possible and have been conducted successfully (e.g. Oerter et al., 2017; Quade et al., 2019; Künhammer et al.,2021), but require uninterrupted AC power, adequate shelter as well as safe and stable operating environments for best results. These prerequisites are not often available at most field sites, especially in more remote locations and for longer sampling time frames.

Second, the testing and adoption of vapor permeable tubing provides a way to sample soil water vapor with minimal disturbance to the soil profile (e.g. Rothfuss et al., 2013; Quade et al., 2018; Oerter and Bowen, 2019; Beyer et al., 2020; Kubert et al., 2020). This method works by flushing dry nitrogen (or dry air) through the vapor permeable membrane (Accurrell PP V8/2HF, 3M, Germany), creating a water vapor gradient from inside the probe to the soil, thus inducing water vapor movement across the membrane. Water vapor is then entrained in the dry nitrogen and flushed to either a CRDS system or into a storage container. The adoption of vapor permeable tubing has been a large step forward for the ecohydrology community, and opened the possibility of creating long-term soil water stable isotope records, particularly when paired with measurement in the field by spectroscopic instruments. While this application is a major advancement, it has many practical limitations for remote field sites, therefore, we aimed to develop a system, termed the SWISS, that is capable of independently collecting samples and can then store those samples for a period of time before being returned to the lab for analysis.

2.1 Soil Water Isotope Storage System details and previous work

The Soil Water Isotope Storage System (SWISS) uses three basic components for water vapor storage of multiple samples: glass flasks, stainless steel tubing and a flask selector valve (Fig. 1, Supplementary Table 1). The ability of the SWISS to reliably store water vapor for up to 30 days was demonstrated previously using a series of lab experiments (Havranek et al., 2020). This proof of concept demonstrated that the flasks retain original water isotope values, but the laboratory system was not field deployable or have customizable automation. Here, we present a fully autonomous, field-ready system that has been thoroughly tested under both laboratory conditions and field conditions, including development and testing of a solar-powered, battery backed automation system that enables pre-scheduled water vapor sampling without manual intervention in remote field locations.

2.2 Field Sites:

2.2.1 Site Set-Up

In figure 1 we show the field-setup employed at all of our field sites. At each site we dug two holes. One hole is instrumented with soil moisture and temperature data loggers at 25 cm, 50 cm, 75 cm, and 100 cm depths, as well as the water vapor permeable probes at 25 cm, 50 cm and 75 cm depths (Fig 1A). All probes were deployed >9 months before the first samples were collected to allow the soil to settle and return to natural conditions as much as possible. During probe deployment we took care to retain the original soil horizon sequence and horizon depths as

106
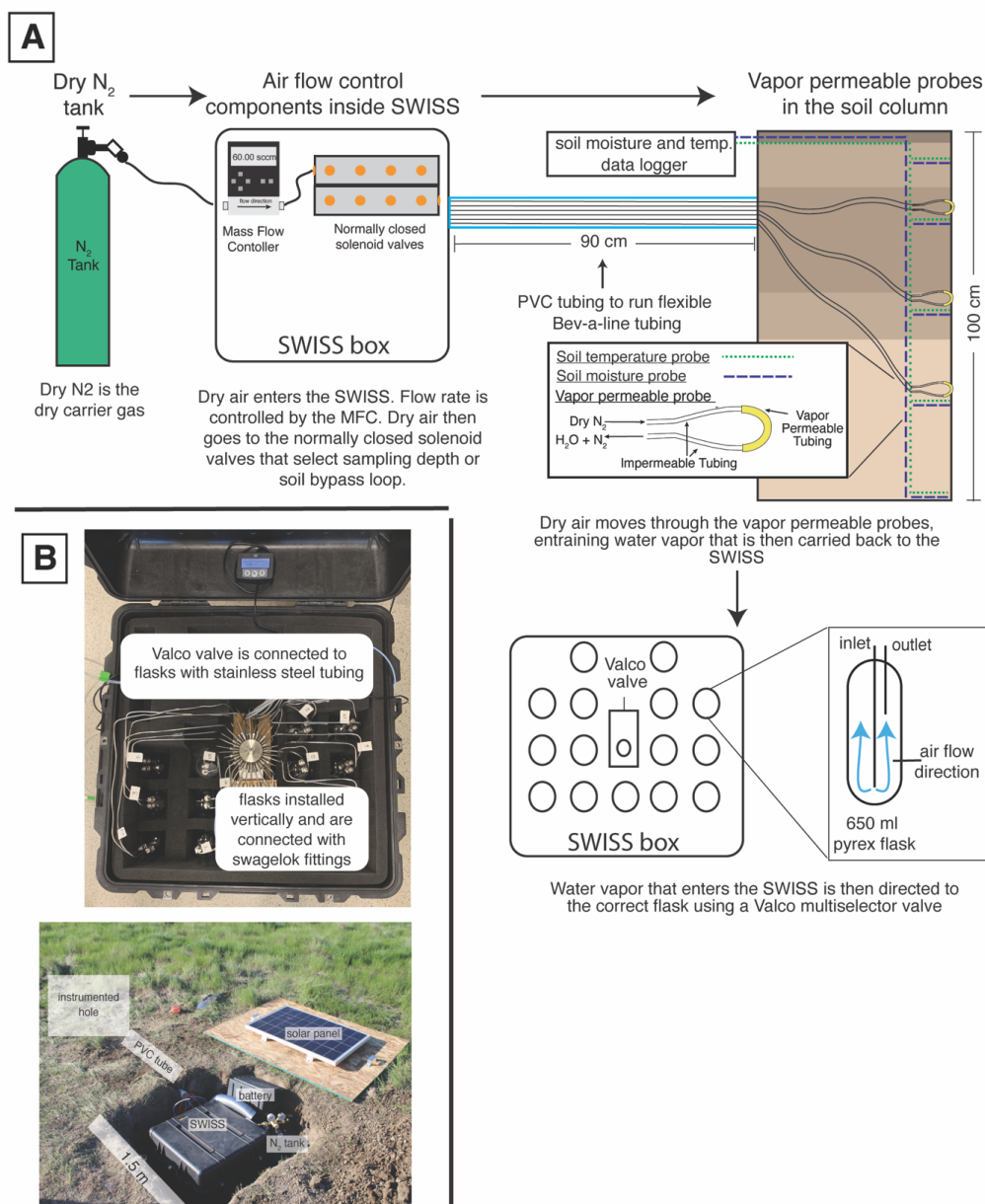
Figure 1. A) The sampling flow path. To sample soil water, dry nitrogen is regulated at a specific rate using a mass flow controller, and then directed to one of the three sampling depths, or the soil bypass loop using a set of solenoid valves. Both the mass flow controller and solenoid valves are housed inside the SWISS. Once directed to the correct sampling depth, dry nitrogen is carried to the vapor permeable probes via gas impermeable tubing that is buried approximately 15 cm depth. After passing through the vapor permeable probe, the entrained soil water vapor is carried back to the SWISS where it is directed to the correct flask using a Valco multiselector valve. B) Photos of a built-out SWISS and the layout of a field site. Each of the system components (I.e. solar panel, battery, N2 tank, SWISS, PVC tube) are labeled, in addition to the location of the instrumented hole in which all of the probes are buried. The hole which houses the SWISS, power, and N2 tank is approximately 1.5 m wide.

116

117   much as possible. The second hole is where the SWISS unit, dry nitrogen tank, and associated components to power

118   the SWISS are stored (Fig 1B). The water vapor probes, which connect to the SWISS with Bev-A-Line impermeable

119   tubing, are run through a PVC pipe buried at approximately 15 cm depth. We chose to run the impermeable tubing

120   to the SWISS underground to limit the effect of diurnal temperature variability on the impermeable tubing, so as to

121   limit condensation as water travels from the relatively warm soil to the SWISS.

122

123   **2.2.2 Site description**

124   We deployed the SWISS at three field locations: Oglala National Grassland, Nebraska, USA; Briggsdale,

125   Colorado,USA; and Seibert, Colorado, USA.

126   The Oglala National Grassland site (Lat: 42.9600/Long:, -103.5979/elev: 1117 m) is located in

127   northwestern Nebraska, USA in a cold semi-arid climate. The soil at this site is described as an aridisol with a silt-

128   loam texture. It is part of the Olney series (Natural Resources Conservation Service, 2022).

129   The Briggsdale site (Lat: 40.5947/Long: -104.3190/elev: 1480 m) is located in northeastern Colorado, USA

130   in a cold semi-arid climate. The soil at this site is described as an alfisol with a loamy sand - sandy loam texture. It is

131   part of the Olnest series (Natural Resources Conservation Service, 2022).

132   The Seibert site (Lat: 39.1187/Long: -102.9250/Elev: 1479 m) is located in eastern Colorado, USA in a

133   cold semi-arid climate. The soil at this site has been described as an alfisol, that has a sand loam texture in the top 50

134   cm of the profile, and a silt loam texture between 50 - 100 cm. It is part of the Stoneham series (Natural Resources

135   Conservation Service, 2022).

136   **3 Materials**

137   **3.1 SWISS Hardware components**

138   In each SWISS there are 15 custom made ~650 ml flasks. These flasks are designed similarly to those used

139   for other water vapor applications. For example, a similar flask is currently used in an unmanned aerial vehicle to

140   collect atmospheric water vapor samples for stable isotope analysis (Rozmiarek et al., 2021). The flasks have one

141   long inlet tube that extends into the flask almost to the base, and one shorter outlet tube so that vapor exiting the

142   flask is well mixed and representative of the whole flask (Fig. 1A). The large flask volume is advantageous because

143   there is a low glass surface area to volume ratio, and therefore we are able to reliably measure vapor from the flasks

144   on a CRDS instrument without interacting with vapor bound to the flask walls. The 15 glass flasks are connected to

145   a 16-port, multi-selector Valco valve. We chose to use a Valco valve because these have previously been shown to

146   sufficiently seal off sample volumes for subsequent stable isotope analysis (Theis et al., 2004). The valve and flasks

147   are connected by ⅛ inch stainless steel tubing and stainless steel ¼ inch to ⅛ inch union Swagelok fittings; we use

148   PTFE ferrules on the glass flasks with the Swagelok fittings. The first port of the valco valve is 1/8th inch stainless

149   steel tubing that serves as a flask bypass loop, which enables flushing of either dry air or water vapor through the

150   system without interacting with a flask. All components are contained in a 61 cm x 61 cm x 61 cm Pelican case with

151 foam. This case is insulated, and provides enough protection to allow reliable transport of the SWISS by vehicle to
152 field sites.
153
154 **3.2 Soil Probes**
155   There are three components for the collection and interpretation of soil water vapor: vapor permeable
156 probes, soil temperature loggers, and soil moisture sensors (Fig 1B, Supp. Table 1). Here, we use a vapor permeable
157 membrane (ACCURELL PP V8/2HF, 3M, Germany) that was first tested by Rothfuss et al., (2013). We opted to
158 use this tubing because it has been shown to deliver reliable data over time (i.e. Rothfuss et al., 2015), and is easy to
159 use and customize to individual needs. We previously observed that variability in the length of the vapor permeable
160 tubing can lead to systematic offsets in the stable isotope composition of measured waters (Havranek et al., 2020).
161 Therefore, we were careful to construct all probes such that the length of the Accurrell vapor permeable tubing was
162 10 cm long, and the impermeable Bev-A-Line IV connected on each side of the vapor permeable tubing was 2 m
163 long. We also constructed the vapor permeable probes to be used in the lab setting for standards in an identical
164 fashion. Soil temperature loggers (Onset HOBO MX2201), used for applying a temperature correction to all soil
165 water vapor data, were buried at the same depths as the vapor permeable probes. Soil moisture sensors (Onset S-
166 SMD-M005) were also buried at the same depths as the vapor permeable probes.
167
168 **3. 3 Automation components, code style, and remote setting power**
169   The philosophy behind the automation of the SWISS was to make it as easy to reproduce as possible, and
170 as flexible as possible to meet different users' sampling needs. We therefore use widely available hardware
171 components and electronics parts; for each product there are numerous alternatives which should be equally viable
172 and could be swapped to better meet each user's needs. In an effort to make our system as accessible and
173 customizable as possible for the scientific community, all automation code is completely open source and will
174 continue to be refined for future applications and hardware improvements. We note that all code is provided as is
175 and should be tested carefully for use in other experiments.
176   The overall sampling scheme used in this paper is described in figure 2 and table 1. Our experimental goal
177 was to create a time series of soil water vapor data from three discrete sampling depths (25 cm, 50 cm, 75 cm). Prior
178 to sampling any soil water vapor, we flushed away any water vapor present in the lines within the SWISS prior to
179 flushing the sample loops. Then, at the start of sampling for each depth, we also flushed the water vapor probe to
180 remove condensation or 'old' water vapor. The gas from both of those steps was expelled via the flask bypass loop.
181 Each soil depth was then sampled for 45 minutes by flushing through the next flask designated in the sequence.
182   Supplement Figure SI 1 shows the components of the automation system. To automate and program the
183 sampling scheme, we used: (1) a microcontroller to run the automation script; (2) a coin-cell battery powered real
184 time clock so that the microcontroller was always capable of keeping track of time through power losses, and
185 therefore maintain the sampling schedule; (3) an RS-232 to TTL converter for serial communication with the Valco
186 valve; (4) solenoid valves that were used to control which depth was being sampled and the associated VDC power
187 relay; (5) a mass flow controller used to control the rate at which dry nitrogen (1 ppm H_2O) is flushed through the
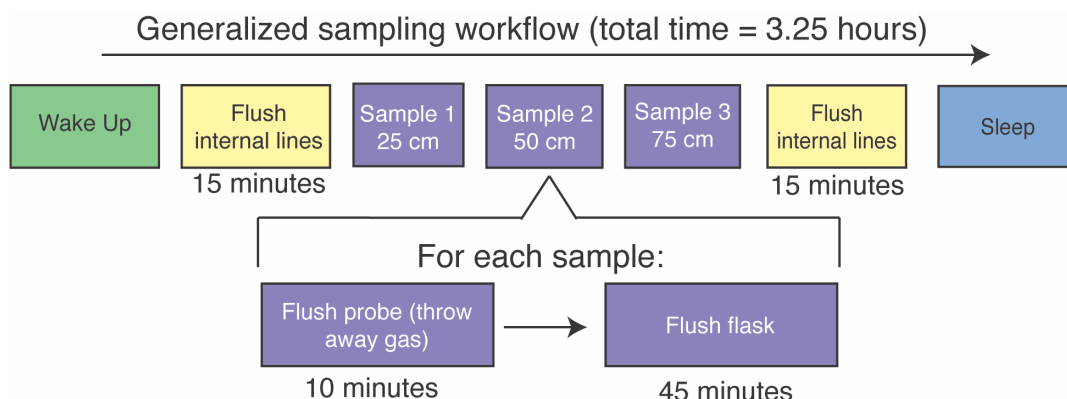
188
189   **Figure 2. Flow chart of the instrument schedule used for sampling during all field experiments.**
190

Code Step	Wake-up	Flush internal lines	Flush depth 1	Sample depth 1	Flush depth 2	Sample depth 2	Flush depth 3	Sample depth 3	Flush internal lines	sleep
time (minutes)	1	15	10	45	10	45	10	45	15	1
Valco valve position	flask bypass	flask bypass	flask bypass	2, 5, 8,11, or 14	flask bypass	3, 6, 9, 12, or 15	flask bypass	4, 7, 10, 13, or 16	flask bypass	flask bypass
solenoid valve position	none	soil bypass	25 cm	25 cm	50 cm	50 cm	75 cm	75 cm	soil bypass	none

191   **Table 1. Description of soil water sampling steps**
192

193   probes; and (6) a power relay used to power the Valco valve and mass flow controller. All parts are described in

194   detail in Supplemental Table 2.

195   In a remote setting, the SWISS units are powered using the combination of a 12V deep-cycle battery and a

196   12VDC, 100W solar panel that is used to charge the battery. The solar panel is mounted to a piece of plywood that

197   covers the hole where the SWISS is deployed (note, the hole is uncovered in Fig. 1B for illustrative purposes). We

198   opted for this setup because the underground storage of all parts of the system creates a discreet field site that

199   attracts minimal attention from other land users. In the field, we used a 12VDC-120VAC power inverter to provide

200   simple plug and play power for the Valco valve and mass flow controller. This simple combination was suitable for

201   summertime in the Western U.S. where there are a great number of sunny hours, and the solar panel was able to

202   easily charge the 12V battery. This setup may need to be adjusted based on location and desired sampling time. Like

203   the automation system, there are many commercial options available for products, and they can be easily adjusted

204   for users' needs; example parts are described in detail in Supplemental Table 2. We also note that in areas where it is

205   possible to plug into a power grid, the deep cycle battery, solar panel and power inverter can be removed.

206

4 Methods

4.1 QA/QC: Testing the SWISS under lab conditions

The highest order concern for the SWISS is that it remains leak-free because any leaks introduce potential for fractionation or mixing of atmosphere that would alter the stable isotope ratio of the water vapor in the flask. So, we developed a three-part quality assurance and quality control (QA/QC) procedure that must be completed for each new SWISS prior to the first deployment. The first step detects any significant leaks using helium detection methods; the second step is to perform a dry air test to detect medium scale leaks; and the third step is to perform a water vapor test to detect slow leaks. Below, we quickly summarize each of these QA/QC steps. Full procedural descriptions are available in supplementary material and the data processing code is available via github.

4.1.1 Step 1: using helium to detect large scale leaks

After initial assembly of the SWISS plumbing, we filled the flasks with helium and used a helium leak detector to find large leaks. Typically, the kinds of leaks we were able to detect with this method were due to cracking of the inlet or outlet on the glass flask that occured while tightening the swagelok fittings. Another easy alternative is to complete a short dry air test (described below) that requires on the order of 12-24 hours.

4.1.2 Step 2: dry air tests detect medium scale leaks

Once we felt sure that there were no major leaks in our systems, we completed a dry air test. The goal of this test was to catch any second order, medium-scale leaks. Typically, this test found swagelok fittings that had been under tightened. The advantage of this kind of test is that it is easy and quick to complete. This test started with a dry air fill. A *dry air fill* consists of flushing flasks with air that is filtered through drierite (which has a water vapor mole fraction of less than 500 ppm), at 2 L/min for 5 minutes. With a flask volume of 650 ml, this means the volume of the flask is turned over 15 times. Flasks were then sealed and left to sit for seven days.

At the end of the seven-day period we measured each flask using the *dead-end pull sample introduction* (note, italicized terms are specific methods, and are explained in greater detail in supplementary material) method on a Picarro L2130-*i* Isotope and Gas Concentration Analyzer. For this sample introduction method, the inlet to the valco valve was sealed with a ¼" swagelok cap and there was no introduction of a carrier gas. As a result, air was removed from the flask based on the flow rate of the Picarro CRDS (typically 27 - 31 ml/min).

We found that in a low-humidity environment, we needed a week to really see leaks, but this timescale would likely be shorter in more humid locations. Additionally, this test could be modified based on available equipment (for example, if an instrument is available to measure trace atmospheric gases, that could be used instead). To ensure that SWISS units continue to operate as expected, this test should be done between field deployments on every SWISS unit.

We repeated dry air tests until the majority (typically at least 13/15) flasks had a water vapor mole fraction value of less than 500 ppm at the end of the seven day experiment. Water vapor values from the CRDS have not been independently calibrated, but relative variations are believed to be reliable.

4.1.3 Step 3: Water vapor tests detect small scale leaks

The purpose of this experiment was to mimic storage of water vapor at concentrations similar to what we might expect in a soil, and for durations similar to those of our field experiments. Additionally, these tests were used to demonstrate that flasks that were filled early in the sampling sequence did not lead by the time the samples were returned to the lab for measurement. For this experiment, flasks were filled with water vapor of known isotopic composition and known concentration, sealed for 14 days, and then we measured the water vapor concentration and isotope values.

Prior to putting any water vapor into the flasks (either in the field or in the lab), we completed a dry air fill (as defined above) that served to purge the flasks of any prior water vapor that might exchange with the new sample.

To supply water vapor to the flasks, we used the vapor permeable tubing immersed in water. Across three different measurement sessions, we used three different waters that are used as tertiary standards in the INSTAAR SIL lab to complete these experiments: a light water made from melting and filtering Rocky Mountain snow (-25.5‰ and -187.5‰ VSMOW, for $\delta^{18}O$ and δ^2H, respectively), an intermediate water that is deionized (DI) water from the University of Colorado Boulder Campus (~-16.2‰ and -120.7‰ VSMOW for $\delta^{18}O$ and δ^2H, respectively) and a heavy water that is filtered water sourced from Florida, USA (~ -0.8‰ and -2.8‰ VSMOW for $\delta^{18}O$ and δ^2H, respectively). All secondary lab standards are characterized relative to international primary standards obtained from the International Atomic Energy Agency and are reported relative to the V-SMOW/SLAP standard isotope scale. We flushed the flasks at a rate of 150 ml/min for 30 minutes, and measured the $\delta^{18}O$ and δ^2H values and mole fraction of water vapor as each flask was filled. To calculate the input value, we averaged $\delta^{18}O$ and δ^2H over the last three minutes of the filling period.

At the end of the 14-day storage period, we measured each flask to evaluate if the isotope composition had significantly changed over the storage period. To mitigate memory effects between flasks, we ran dry air via the flask bypass loop (port 1 of every Valco valve) for 5 minutes between each flask measurement. During this 5 minute window, we used a heat gun to manually warm each flask. The purpose of the heating was to help create a longer, more stable window of measurement time. While the temperature of the flask was not strictly controlled or regulated, they were all warm to the touch.

Once the flask was warmed and the impermeable tubing dried, water vapor was introduced to the CRDS using one of two methods: 1) the dead-end pull method described above, or 2) a *dry air carrier gas sample introduction* method. The dead-end pull method is preferable when the water vapor mole fraction inside the flask is low (<17,000 ppm). But, the major downside of the dead-end pull method is that condensation forms in the stainless steel tubing that connects the flasks to the Valco valve, as well as the Valco valve itself, far more commonly as compared to the *dry air carrier gas method*. During the dry air carrier gas method, dry air is continuously flowing through the flask at a rate of 27-31 ml/min for the entire 12 minute measurement period. Additionally, to reach a water vapor mole fraction of approximately 25,000 ppm (the optimal humidity range for the CRDS), we diluted the water vapor with dry air at a rate of 10 ml/min. Without dilution, the concentration out of the flasks is as high as 35,000 - 40,000 ppm, which leads to saturation issues on a Picarro L2130-*i*. Providing a carrier gas prevents condensation from forming in the Valco valve and tubing, and prevents fractionation that may occur because of

281 changing pressure within the flask. The dry air carrier gas method is our preferred method for sample introduction in
282 most cases.
283   For each flask we looked at signal stability individually, and for approximately 90% of the flasks we found
284 that after excluding the first three minutes of measurement of each flask, the subsequent three minutes were the most
285 stable and consistent. For some flasks, using either a later portion of the measurement period, or slightly earlier
286 offered a more stable signal.
287   During these experiments, instrument drift and stability were monitored using a suite of four waters of
288 known composition that were introduced to the CRDS using a flash evaporator system, described in detail by
289 Rozmiarek and others (2021). Additionally, instrument stability was assessed by measuring water vapor of known
290 composition that was produced using the vapor probes, in a fashion that is identical to how the flasks were flushed.
291
292 **4.2 Field suitability and Field application experiments:**
293 **4.2.1 Field suitability experiment #1: Long term field leak test**
294   As a complement to the QA/QC we did under lab conditions, we also completed long term dry air tests at
295 our field sites. The purpose of these experiments was to demonstrate that even under field conditions the flasks are
296 still resistant to atmospheric intrusion. Furthermore, this leak test was used to demonstrate that the flasks filled last
297 during the sampling sequence had not taken on an atmospheric isotope composition prior to sampling.
298   Like all field deployments, we started with a dry air fill, and then one SWISS was deployed to each of our
299 three field sites. No soil water was collected during these deployments. The duration between filling the flasks with
300 dry air to measuring the flasks was anywhere between 34 - 52 days.
301
302 **4.2.2. Field suitability experiment #2: Mock field tests**
303   To demonstrate that the automation code and sampling scheme we propose worked as expected on short,
304 observable timescales, we set up an experiment to simulate field deployment of one SWISS unit (Meringue) near the
305 University of Colorado Boulder. This test used the automation components and remote power setup described in the
306 materials section. During this field-simulation experiment, our goal was to collect three discrete samples each
307 sampling period, to simulate collection of samples from three depths at each field site. Importantly, we wanted to
308 demonstrate that the sampling scheme does not introduce significant memory effects between samples.
309   Over the course of 25 hours, all 15 flasks were filled with three different vapors. Two were water vapors,
310 created from the light water and intermediate water as described above in the water vapor test section. The third was
311 water vapor from the ambient atmosphere. For this experiment we filled three flasks per cycle with each one of the
312 waters (e.g. Flask 2 = light, Flask 3 = intermediate, Flask 4 = Atmosphere).
313   For seven days, the SWISS unit was stored in a simulated field setting, while the water vapor remained in
314 the flasks. At the end of the seven days, flasks with a higher water vapor mole fraction (light and intermediate water
315 vapor samples) were measured using the carrier gas sample introduction method, whereas those with a low water
316 vapor mole fraction (atmosphere) were measured using the dead end pull sample introduction method. We used
317 equations 2A and 2B from Rothfuss et al., (2013) to convert from water vapor to liquid values. Then, using tertiary

318   standards, data were corrected into the VSMOW data frame. Finally, the SWISS unit offset correction (detailed

319   below) was applied.

320

321   **4.2.3 Full field deployment experiment: One month period**

322   We deployed one SWISS unit each to the three field sites described. We sampled at three depths (25 cm, 50

323   cm, and 75cm) on each sampling day, following the protocol in figure 2. We sampled at each depth every 5 days

324   (protocol length = 25 days total). At the end of a 28 day period, the SWISS units were returned to the lab, and

325   measured. The measurement protocol and data reduction protocol follows the procedures described in the water

326   vapor QA/QC test section above. The data correction scheme follows as in the section above.

327   **5 Results**

328   **5.1 QA/QC Results**

329   **5.1.1 Dry air test**

330   Figure 3 shows the results of a seven-day dry air test for three SWISS units (marked by the box name) (SI

331   Table 3). For all three SWISS units, at least 13/15 of the flasks maintained a water vapor mole fraction value of less

332   than 500 ppm over the seven day period. In two of the three SWISS units (Lindt and Raclette), the water vapor mole

333   fraction for flasks was randomly distributed around approximately 350 ppm. In Toblerone there was a systematic

334   decrease in water vapor mole fraction from flask 2 through flask 16, matching the order in which the flasks were

335   filled with dry air initially. In both Lindt and Toblerone, flask 2 had the highest water vapor mole fraction of all the

336   flasks.
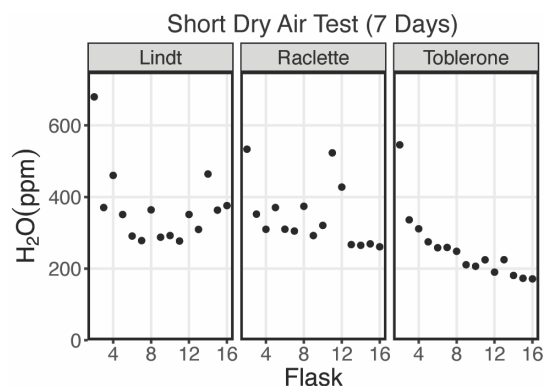
337

338   **Figure 3. Results of a dry air test from three different SWISS units named: Lindt, Raclette and Toblerone. The majority**
339   **of the flasks maintain a water vapor mixing ratio of less than 500 ppm.**
340

341   **5.1.2. Water vapor test**

342   In panels a and b of figures 4 and 5, we show the results of 11 different water vapor tests performed across

343   three analytical sessions using 6 different SWISS units. This dataset includes water vapor tests using three different

344   water vapors (light, intermediate and heavy) and uses both the dead-end pull and dry-air carrier gas methods to

345   introduce water vapor to the CRDS. Across these three sessions, we measured 164 flasks while filling them with

346   water vapor and at the end of the two week hold period. After correcting for instrument drift, we calculated the

347   difference between the starting and end values to assess drift in water vapor isotope values due to leaking or other

348   measurement bias.

349   Ideally, we expect a normal distribution centered about 0 within the uncertainty limits of the water vapor

350   probes (Oerter et al., 2016). For $\delta^{18}O$, the mean difference between the start and end values for the flasks is 1.1‰

351   with a standard deviation of 0.72‰ (outliers removed). There is a consistent positive offset, with a few clear outliers

352   (Fig. 4A). We do not observe a consistent difference between water vapor sample introduction methods (Supp. Fig.

353   2). After removing outliers (< Q1 - 1.5*IQR or > Q3 + 1.5*IQR, n = 15) from the dataset, we compared the kernel

354   density estimate shape to a normal distribution calculated from the mean and standard deviation of the dataset to

355   assess dataset normality (Fig. 4B). A normal distribution slightly overestimates the center of the data, but captures

356   the overall shape fairly well. Therefore, we used the median offset (1.0‰) to correct our water vapor isotope values,

357   and used the interquartile range of the dataset (outliers removed) to estimate uncertainty of the SWISS as ± 0.9‰ .

358   In figure 5C, for simplicity, we just present the results from 45 flasks (three SWISS units), with the 1.0‰ offset

359   correction applied. After correction, data are randomly distributed about 0, and are within the uncertainty range of ±

360   0.9‰ (Supp. Table 4).

361   For δ^2H, the mean difference between the start and end values is 2.63‰ with a standard deviation of 2.85‰

362   (outliers removed). Similarly to $\delta^{18}O$, we ideally expected a normal distribution of differences centered around 0. As

363   with $\delta^{18}O$, there was a consistent positive offset with some outliers (i.e. < Q1 - 1.5*IQR or > Q3 + 1.5*IQR) (Fig.

364   5A). After removing outliers (n = 26) from the dataset, we compared the kernel density estimate to a normal

365   distribution calculated from the mean and standard deviation of the dataset to assess dataset normality (Fig. 5B). As

366   for $\delta^{18}O$, the center of the dataset is overestimated by the mean, but the overall peak shape is roughly captured. We

367   therefore use the median value of 2.3‰ as an offset correction, and estimate uncertainty at ±3.7‰ for δ^2H from the

368   interquartile range. In figure 5C, we present the results from 45 flasks (three SWISS units), with the 2.3‰ offset

369   correction applied. Data are randomly distributed about 0, and are within the uncertainty range of ± 3.7‰ (Supp.

370   Table 4).

371

372   **5.2 Field suitability and field deployment experiment results**

373   **5.2.1. Dry air test**

374   Figure 6A shows the result of placing SWISS units that were flushed with dry air out into field conditions

375   over the course of 34 - 52 days (SI Table 3). We chose these time intervals because they bracket the typical length of

376   a deployment, which helped us determine how quickly flasks should be measured after bringing a SWISS back to

377   the lab. At the timescale of 34 - 43 days, 13 of the 15 flasks typically maintained a water vapor mole fraction of less

378   than 1000 ppm. At the timescale of 52 days, eight of the 15 flasks had a water vapor mole fraction between 1000 -

379   2500 ppm, and the remaining seven flasks had a water vapor mole fraction of less than 1000 ppm. Given that these

380   tests were completed with different SWISS units, these data also include some of the inter-unit variability.

381

382
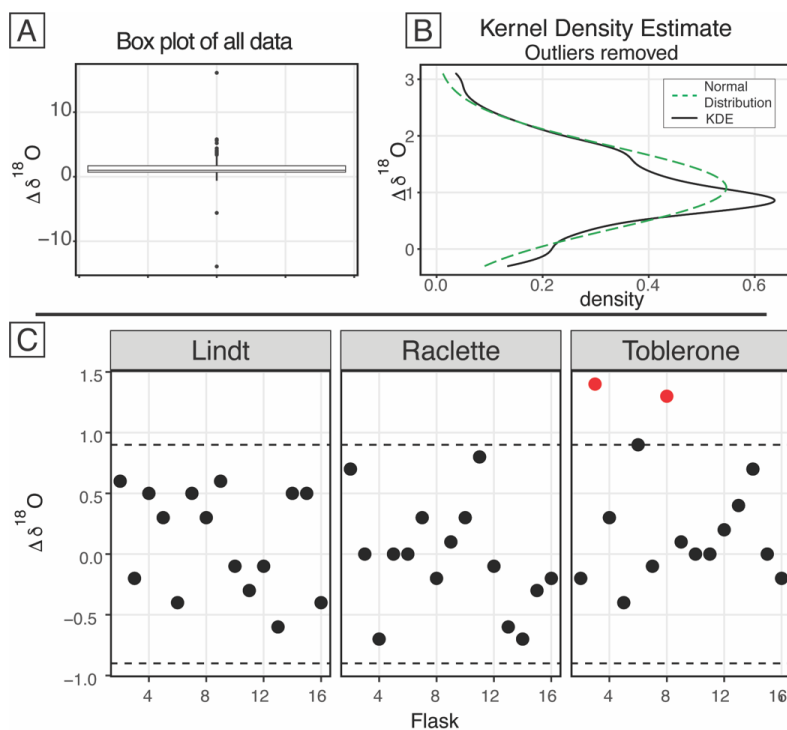
Figure 4. Results of the water vapor tests. A) Boxplot of the difference between the starting $\delta^{18}O$ value and the final $\delta^{18}O$ value of all 164 flasks. B) After removing the outliers from the dataset, the kernel density estimate (black line) and the normal distribution calculated from the dataset (dashed green) are shown. C) After applying the offset correction of 1.0‰, the difference between the starting $\delta^{18}O$ value and the final $\delta^{18}O$ value for three boxes from the August 2022 session are shown. An uncertainty of ± 0.9‰ is marked with a dashed line, and data points that fall outside that uncertainty are colored red.

411

412
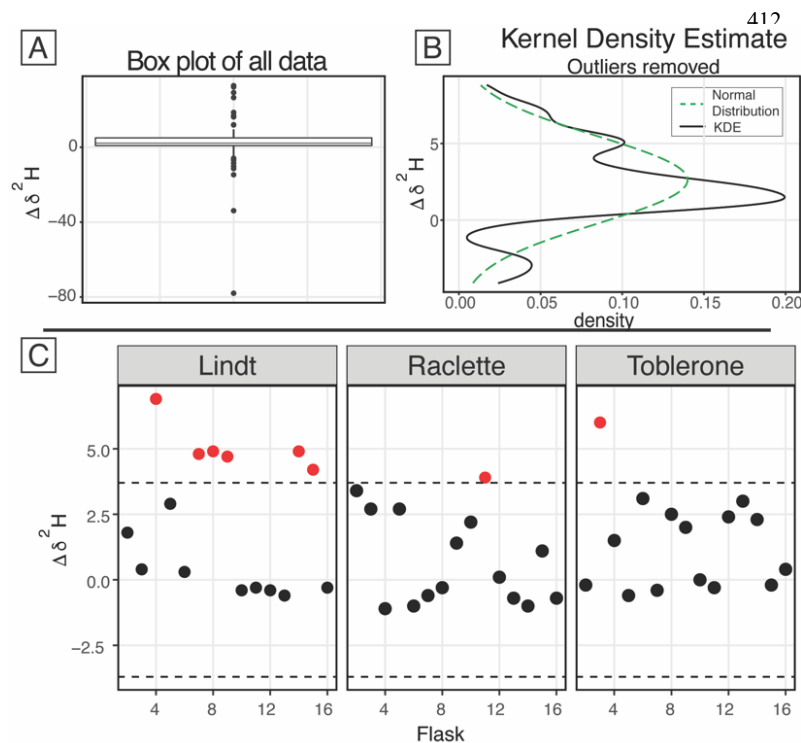
Figure 5. Results of the water vapor tests A) Boxplot of the difference between the starting δ^2H value and the final δ^2H value of all 164 flasks. B) After removing the outliers from the dataset, the kernel density estimate (black line) and the normal distribution calculated from the dataset (dashed green) are shown. C) The difference between the starting δ^2H value and the final δ^2H value for three boxes from the August 2022 session are shown after applying the offset correction of 2.3‰. An uncertainty of ± 3.7‰ is marked with a dashed line, and data points that fall outside that uncertainty are colored red.
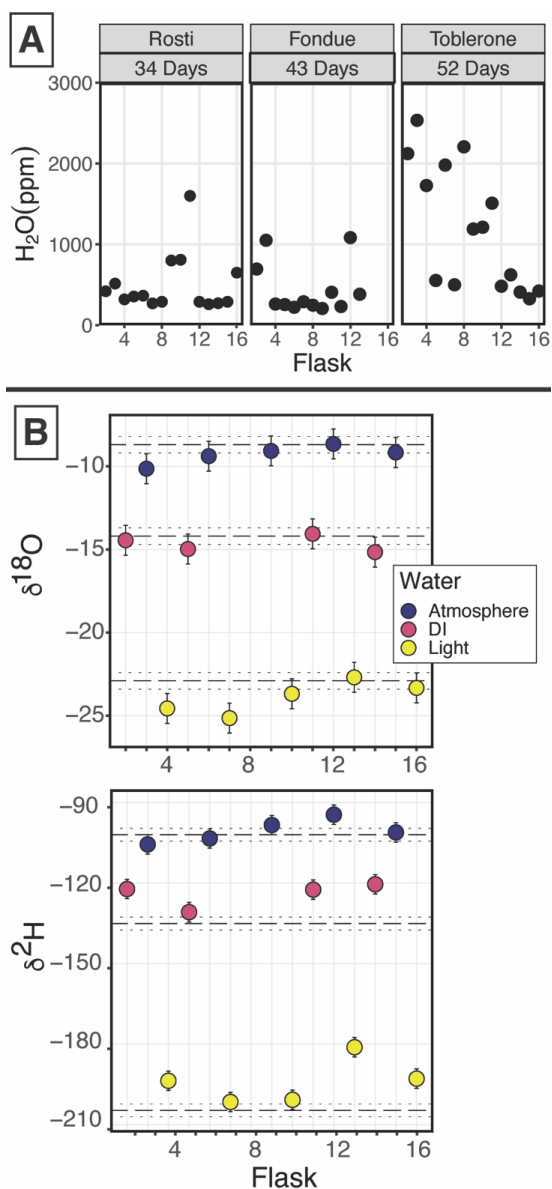
Figure 6. A) Results from three different field-based long dry air tests. B) Results from the automation field suitability tests using the SWISS unit named Meringue. Flasks that sampled atmosphere are shown in blue, flasks that sampled deionized water (DI) are shown in pink, and flasks that sampled the light water are shown in yellow. The top plot shows the $\delta^{18}O$ results, and the bottom plot shows the δ^2H results.

490

491
492

493

494

495

496

497

498 **5.2.2. Automation test**

499   Figure 6B shows the result of using the automation code to collect and store water vapor of known

500 composition for seven days (Table 2). In both plots, the known values of the water are shown as a long-dash line.

501 Uncertainty on those measurements is estimated at 0.5‰ and 2.4‰ for $\delta^{18}O$ and δ^2H respectively (Oerter et al.,

502 2016), shown as the dotted lines. We estimated the isotope value of the atmosphere at the time of sampling with data

503 from the CRDS in the lab. The corrected isotope value of each flask is shown, with uncertainty associated with the

504 SWISS units estimated at 0.9‰ and 3.7‰ for $\delta^{18}O$ and δ^2H, respectively.

505   Seven of the nine flasks filled with water vapor overlap within uncertainty of the known $\delta^{18}O$ value for

506 those standards (top plot, Fig. 6B), and four of the five flasks filled with atmospheric vapor overlap within

507 uncertainty of our estimated $\delta^{18}O$ value. Flasks that fall outside of the bounds of uncertainty tend to have lower $\delta^{18}O$

508 values than the expected value. For δ^2H, (bottom plot, Fig. 6B) only three of the nine flasks filled with water vapor

509 overlap within uncertainty of the known value of those standards, while four of the five flasks filled with

510 atmospheric vapor overlap within uncertainty of the estimated δ^2H value. Flasks that fall outside of the bounds of

511 uncertainty typically have higher δ^2H values than the expected value.

512

SWISS	Flask	water	$\delta^{18}O$ (‰)	δ^2H (‰)
Meringue	2	DI	-14.4	-122.2
Meringue	3	Atmosphere	-10.1	-105.6
Meringue	4	Light	-24.6	-193.7
Meringue	5	DI	-15.0	-130.8
Meringue	6	Atmosphere	-9.4	-103.4
Meringue	7	Light	-25.1	-201.5
Meringue	8	DI	-17.3	-140.5
Meringue	9	Atmosphere	-9.1	-98.4
Meringue	10	Light	-23.7	-200.7
Meringue	11	DI	-14.1	-122.5
Meringue	12	Atmosphere	-8.7	-94.5
Meringue	13	Light	-22.7	-181.2
Meringue	14	DI	-15.2	-120.5
Meringue	15	Atmosphere	-9.2	-101.1
Meringue	16	Light	-23.3	-192.9

513 **Table 2. Results of the Automation test**

514

515 **5.2.3 Field deployment**

516   Figure 7 shows the results from three field deployments in Oglala National Grassland, Nebraska;

517 Briggsdale, Colorado; and Seibert, Colorado (table 3).

518
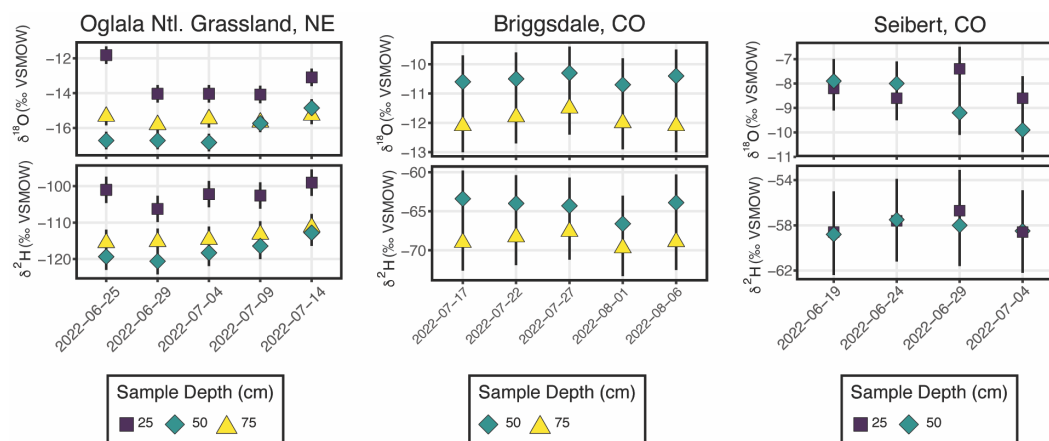
Figure 7. Results from all three field deployments to Oglala National Grassland, NE, Briggsdale, CO and Seibert, CO. Note, the y-axis scale for all three plots is different.

There are 15 samples from Oglala National Grassland (Fig. 7); five from 25 cm depth, five from 50 cm depth and five from 75 cm depth. Samples were taken approximately every five days from 2022-06-25 to 2022-07-14. Four of the five samples from 25 cm overlap within uncertainty in δ^{18}O value, and all five samples overlap with uncertainty in δ^{2}H value.There is a significant decrease in the δ^{18}O value at 25 cm between 2022-06-25 and 2022-06-29. There is no similar shift in δ^{2}H value over the same time period. The first three samples from 50 cm overlap in both δ^{18}O and δ^{2}H values, then the final two samples drift to higher isotope values. All five samples from 75 cm overlap in δ^{18}O and δ^{2}H values. Similar to the samples from 50 cm, there is a trend towards higher δ^{2}H values for the last three samples. Overall, δ^{18}O and δ^{2}H values from 25 cm are significantly higher than the values from 50 and 75 cm depth. Generally, samples from 50 cm depth have lower δ^{18}O and δ^{2}H values than samples from 75 cm depth.

There are 10 samples from Briggsdale, CO (Fig. 7); five samples are from a vapor probe buried at 50 cm depth and five samples are from a vapor probe buried at 75 cm depth. Data from 25 cm at Briggsdale, CO were excluded because the water vapor mole fraction from all of the flasks with samples at this depth had extremely low water vapor mole fractions (<13,000 ppm), and so those data may either represent atmosphere or soil gas from an extremely dry soil. Samples were taken every five days between 2022-07-17 and 2022-08-06. All samples overlap within uncertainty in both δ^{18}O and δ^{2}H values, however samples from 50 cm are clearly offset to higher values for both δ^{18}O and δ^{2}H as compared to samples from 75 cm.

There are 8 samples from Seibert, CO (Fig. 7); four samples are from a vapor probe buried at 25 cm depth and four samples are from a vapor probe buried at 50 cm depth. Samples collected from 75 cm depth at Seibert, CO were discarded because there were significant problems with condensation while measuring these flasks, and so all data were considered spurious. Samples were collected every five days between 2022-06-19 and 2022-07-04. At 25 cm depth, δ^{18}O values of three of the four samples overlap within uncertainty; the 25 cm sample from 2022-06-29 that does not overlap has a higher δ^{18}O value than the other three samples. At 25 cm depth, δ^{2}H values overlap

545   within uncertainty for all four samples. At 50 cm depth, there is a steady decrease in δ^{18}O value over the sampling

546   period, while δ^2H values for all four samples remain steady.

547

548   **6 Discussion**

549   **6.1 QA/QC and field suitability tests**

550   **6.1.1 Dry Air tests**

551   For the seven day dry air tests, the flasks were able to maintain a water vapor mole fraction typically less

552   than 400 ppm, and all flasks maintain a water vapor mole fraction of less than 700 ppm (Fig. 4). In Colorado, the

553   ambient atmosphere during the summertime typically sits at a water vapor mole fraction between 10,000 - 20,000

554   ppm, and in winter the water vapor mole fraction can drop as low as 4000 ppm. If the flasks allowed in a significant

555   amount of atmosphere, the flasks would have had much higher water vapor molar fractions. This suggests that the

556   system is resistant to atmospheric intrusion.

557   There seems to be a systemic bias towards a high water vapor mole fraction for the first flask that is

558   measured (flask 2). There are two potential analytical sources of this. First, its possible that during the filling phase,

559   not all of the atmospheric vapor has been flushed out of the system before starting the fill process. Similarly, it is

560   possible that not all of the atmospheric water vapor was flushed from the line that connects to the CRDS prior to the

561   start of the measurements.

562

563   **6.1.2 Water vapor tests**

564   The in-lab water vapor tests served three functions: 1) they allowed us to test the best method for

565   measuring soil water vapor at fairly high water vapor mole fractions that might be representative of field conditions

566   (i.e. > 25,000 ppm), 2) to test if there is any systemic bias introduced through the building materials or measurement

567   schema, and, 3) test whether soil water vapor samples can yield reliable stable isotope values.

568   We completed 11 water vapor tests using 6 SWISS units and three analytical sessions, resulting in 164

569   measurements of water vapor. Across the three analytical sessions, three waters with different isotopic compositions

570   were used to produce water vapor (1 heavy, 1 intermediate, and 1 light). If there was alteration of original values due

571   to leaky flasks, we might expect the δ^{18}O and δ^2H values to converge on the δ^{18}O and δ^2H value of the atmosphere.

572   For example, we might expect water vapor from the light water test to have the most significant change in isotope

573   value, towards that of the ambient atmosphere.

574   Figures 4 and 5 demonstrate that there is a consistent offset in both δ^{18}O and δ^2H of the water vapor from

575   the start of storage to the end for all three analytical sessions. After removing outliers from the dataset, there remains

576   a consistent bias across all SWISS boxes and analytical sessions (Figs 5B, 6B). The consistency across >135 flasks,

577   different starting water vapor isotope values, sample introduction methods, and multiple analytical sessions suggests

578   that this difference is a function of the storage and measurement. Additionally, the normality of the distribution

579

Site	Date	Sample Depth (cm)	Flask	T	δ¹⁸O (‰)	δ¹⁸O (‰) Analytical Error	δ²H (‰)	δ²H (‰) Analytical Error
Briggsdale	7/17/22	50	3	23	-10.6	0.2	-63.4	0.6
Briggsdale	7/17/22	75	4	23	-12.1	0.2	-69	0.7
Briggsdale	7/22/22	50	6	23	-10.5	0.3	-64	0.7
Briggsdale	7/22/22	75	7	23	-11.8	0.2	-68.3	0.6
Briggsdale	7/27/22	50	9	23	-10.3	0.3	-64.3	0.6
Briggsdale	7/27/22	75	10	23	-11.5	0.2	-67.6	0.7
Briggsdale	8/1/22	50	12	23	-10.7	0.2	-66.6	0.7
Briggsdale	8/1/22	75	13	23	-12	0.2	-69.7	0.7
Briggsdale	8/6/22	50	15	23	-10.4	0.2	-63.9	0.6
Briggsdale	8/6/22	75	16	23	-12.1	0.2	-68.9	0.7
Seibert	6/19/22	25	2	23	-8.2	0.2	-58.6	0.6
Seibert	6/19/22	50	3	23	-7.9	0.2	-58.8	0.6
Seibert	6/24/22	25	5	23	-8.6	0.2	-57.6	0.7
Seibert	6/24/22	50	6	23	-8	0.2	-57.5	0.7
Seibert	6/29/22	25	8	23	-7.4	0.2	-56.7	0.6
Seibert	6/29/22	50	9	23	-9.2	0.2	-58	0.7
Seibert	7/4/22	25	11	23	-8.6	0.2	-58.6	0.7
Seibert	7/4/22	50	12	23	-9.9	0.2	-58.5	0.6
Oglala Ntl. Grassland	6/25/22	25	2	23	-11.8	0.2	-101.0	0.7
Oglala Ntl. Grassland	6/25/22	50	3	22.8	-16.7	0.2	-119.3	0.7
Oglala Ntl. Grassland	6/25/22	75	4	21.5	-15.3	0.2	-115.5	0.8
Oglala Ntl. Grassland	6/29/22	25	5	25	-14.0	0.2	-106.2	0.7
Oglala Ntl. Grassland	6/29/22	50	6	22.8	-16.7	0.2	-120.6	0.7
Oglala Ntl. Grassland	6/29/22	75	7	21.3	-15.8	0.2	-115.2	0.7
Oglala Ntl. Grassland	7/4/22	25	8	25	-14.0	0.2	-102.2	0.7
Oglala Ntl. Grassland	7/4/22	50	9	23	-16.8	0.2	-118.3	0.6
Oglala Ntl. Grassland	7/4/22	75	10	22	-15.5	0.2	-114.7	0.6
Oglala Ntl. Grassland	7/9/22	25	11	23	-14.1	0.2	-102.6	0.6
Oglala Ntl. Grassland	7/9/22	50	12	22.8	-15.7	0.2	-116.4	0.7
Oglala Ntl. Grassland	7/9/22	75	13	22	-15.7	0.2	-113.2	0.6
Oglala Ntl. Grassland	7/14/22	25	14	23	-13.1	0.2	-99.0	0.6
Oglala Ntl. Grassland	7/14/22	50	15	22.8	-14.9	0.3	-112.8	0.7
Oglala Ntl. Grassland	7/14/22	75	16	22	-15.3	0.2	-111.2	0.7

580   **Table 3. Results from the three field deployments of SWISS.**

581

582   suggests that there is a systematic bias that we can reliably correct for. We chose to use the median value as an offset
583   correction over the mean of the normal distribution, because the median is not biased by higher isotope difference
584   values that are a complex combination of systematic bias and slow leaking. The calculated average offset is 1.0‰
585   and 2.6‰ for $\delta^{18}O$ and δ^2H, respectively.
586   Based on the results of the water vapor tests, we estimate the uncertainty of the SWISS at 0.9‰ and 3.7‰
587   for $\delta^{18}O$ and δ^2H, respectively using the interquartile range (IQR) of the water vapor test results after removing
588   outliers from the dataset. We prefer the IQR over the calculated standard deviation of the normal distribution,
589   because IQR is not biased by outlier values. In figures 5C and 6C, we show the results of 3 water vapor tests from
590   the August 2022 analytical session, with an offset correction applied. 43 of the 45 measured flasks faithfully retained
591   the starting $\delta^{18}O$ value of the water vapor, and 37 of the 45 measured flasks faithfully retained the starting δ^2H value
592   of the water vapor. Additionally, after the offset correction was applied, most flasks also fall within the uncertainty
593   of the water vapor permeable probes ($\delta^{18}O$ = 0.5‰ and δ^2H = 2.4‰).
594   Supplemental figure 3 shows a kernel density estimate plot of the results from two water vapor test
595   sessions, with the offset correction applied. During the March 2022 session, flasks were measured using the dead-
596   end pull sample introduction method and during the August 2022 session, flasks were measured using the dry air
597   carrier gas sample introduction method. There is no significant difference in the measured difference between the
598   two sample introduction methods. We prefer the dry air carrier gas method, because it is far simpler to control the
599   water vapor mixing ratio, and optimize the concentration to be around 25,000 ppm, which is the concentration at
600   which the Picarro L2130-i is most reliable. The dry air carrier gas method also makes it far easier to control for and
601   monitor for condensation in the stainless steel tubing and vapor impermeable tubing, which can bias a measurement.
602
603   **6.1.3 Field suitability tests**
604   In Figure 7A, we observe that the flasks typically maintained a low water vapor mole fraction (< 1000
605   ppm) under field conditions, and at timescales relevant to 4-6 week field deployments (34 - 43 days). The 34 day
606   test was done during June 2022, and therefore tests the SWISS under warm summertime conditions. The 43 day test
607   was done in October 2021, which included nights where temperatures fell below 0°C, and therefore tests the
608   suitability of the SWISS to maintain integrity under freezing conditions. We observe that the SWISS did
609   considerably worse at maintaining a low water vapor mole fraction over a 52 day time period during similar
610   summertime conditions as compared to the 34 - 43 day time period. Over the 52 days, seven flasks maintained a
611   water vapor mole fraction less than 1000 ppm and the remaining 8 had a water vapor mole fraction between 1000 -
612   2500 ppm. Though the SWISS performed considerably worse after 52 days than it did from 34 - 43 days, it is
613   important to note that the atmospheric water vapor mole fraction during the storage time period was likely 15,000 -
614   20,000 ppm, and so the measured values demonstrate that the SWISS are still quite resistant to atmospheric intrusion
615   at that timescale.
616   In figure 7B, the data show that the flasks faithfully preserved the $\delta^{18}O$ value of both water vapor produced
617   using the vapor permeable probe and the atmosphere over a seven day period. One flask was removed from the
618   dataset (flask eight), because there was noticeable condensation in the impermeable tubing during the measurement

619   phase, with an increase of > 5‰ for δ^{18}O during the measurement period. Notably, the two flasks whose δ^{18}O

620   oxygen isotope values do not overlap within uncertainty are more negative than expected, rather than drifting

621   towards atmospheric values or values expected with kinetic fractionation. It is possible that those samples were also

622   affected by condensation at the start of the experiment; during condensation, we expect that ^{18}O will preferentially

623   go into the liquid phase, and that the water vapor that enters the flask will have a lower than expected δ^{18}O value.

624   Surprisingly, only 3 flasks filled with either DI or light water vapor overlap within uncertainty of the

625   known δ^{2}H values, while four of the five flasks overlap within uncertainty of the estimated atmosphere isotope

626   value. The flasks tend to drift towards the value of the atmosphere, but retain the overall data pattern from the

627   oxygen isotope values.

628

629   **6.1.4 Lessons learned and recommendations from the QA/QC and field suitability tests:**

630   The dry air test is a time-efficient method for identifying flasks that are leaky and will not preserve the

631   sampled water vapor value, therefore we recommend these tests as a required step prior to field deployment of future

632   SWISS units. For example, supplemental figure 4 shows that it is possible to drastically reduce the water vapor mole

633   fraction in a flask filled with dry air between tests by tightening and/or replacing problematic fittings (both those

634   attached to the glass flasks and those on the valco valve) and in some cases the glass flask itself. This shows we can

635   reduce the leakiness of the flasks. The dry air test is also an easy baseline test that also allowed us to test building

636   materials. For example, in supplemental figure 5, we tested using PTFE swagelok fittings with ⅛" PTFE tubing

637   rather than stainless steel. These materials would be advantageous because they are much easier to install and are

638   significantly lighter. We found that these fittings and tubing *may be* sufficient to store water for up to a single week,

639   but on longer timescales (e.g. 27 days) we observed greater exchange and leaking than the stainless steel. We

640   encourage any future user using this modification to rigorously test these fittings on a timescale appropriate for their

641   application.

642   From the water vapor tests, we get a sense of the accuracy and precision of the SWISS. The calculated

643   uncertainty of the flasks (0.9‰ and 3.7‰ for δ^{18}O and δ^{2}H, respectively) is somewhat larger than the uncertainty

644   associated just with the use of the water vapor probes (0.5‰ and 2.4 ‰ for δ^{18}O and δ^{2}H, respectively, Oerter et al.,

645   2016), but is sufficient for many critical zone applications, given the magnitude of seasonal variability that can be

646   observed in natural systems (e.g. Oerter et al., 2017; Quade et al., 2019).

647   We opted to use a large flask volume because it allows us to measure a sample for long enough on a CRDS

648   that we get reliable data, without interacting with vapor bound to the flask walls. The drawback of this, however, is

649   that we must sample soil water vapor for a relatively long period of time (45 minutes). In supplemental figure 6, we

650   show that the sampling regime, and particularly the length of time we pump dry air through the tubing, does not

651   significantly alter the soil moisture content of the soil. Additionally, we demonstrate that the sampling regime we

652   use does not introduce significant memory effects.

653   Based on the results of the long, field dry air test, we recommend that the water vapor storage time doesn't

654   exceed 40 days for reliable results, or that the user undertake multiple dry air tests with lower concentration

655   benchmarks if deployments may exceed 40 days.

656   Overall, the quality control and quality assurance as well as the field suitability tests demonstrate that the

657   SWISS are able to faithfully retain the isotope value of water vapor collected using water vapor permeable probes.

658   Like many other systems that measure dual isotopes, each system (i.e. $\delta^{18}O$ and δ^2H) must be evaluated separately.

659   In general, we interpret oxygen isotope data with a higher degree of confidence than the hydrogen isotope data. As

660   the automation test revealed however, even when the absolute δ^2H value is not correct, the general pattern can reveal

661   information about soil water dynamics. One particular challenge with the vapor permeable probes, that others have

662   noted, is condensation in any portion of the system (e.g. Quade et al., 2019; Kühnhammer et al., 2019) . As much as

663   possible, it is helpful to have the impermeable tubing at warmer temperatures than the soil or water it is sampling. In

664   many situations it may be worthwhile to warm the transfer tubing, but this should be done in a way that does not

665   alter the thermal structure of the soil, and in remote settings, can operate safely independently. Additionally, taking

666   care to ensure that the SWISS is evenly and lightly warmed in the lab setting helps to prevent condensation from

667   forming in the stainless steel tubing and Valco valve.

668

669   **6.2 Field Deployments**

670   In Figure 7 we show the results of three field deployments completed during summer 2022 (table 3). At the Oglala

671   National Grassland site, we used the SWISS named Lindt to collect samples. During the August 2022 water vapor

672   test on Lindt, all of the oxygen isotope values fall within uncertainty of the system, and nine of the fifteen flasks fall

673   within uncertainty of the system. Therefore, we interpret the $\delta^{18}O$ values with a higher amount of confidence and the

674   δ^2H values with a lower amount of confidence (Figs. 4C and 5C). We note that most of the $\delta^{18}O$ and δ^2H values

675   follow the same trends, and fall on the global meteoric water line (Figs. 7 and 8A). In general, soil water from 25 cm

676   had higher $\delta^{18}O$ and δ^2H values than soil water from both 50 and 75 cm (Fig. 8A). Given that 4 of the 5 samples

677   from 25 cm overlap with the GMWL and have a d-excess that overlaps within error of 10‰, the soil water from that

678   depth may reflect summer precipitation with higher $\delta^{18}O$ and δ^2H values. Soil water from 75 cm had intermediate

679     $\delta^{18}O$ and δ^2H values for most of the study period, and soil water from 50 cm depth had the lowest $\delta^{18}O$ and δ^2H

680   values for most of the study period, which may reflect a more mean-annual or winter precipitation biased value. The

681   d-excess value of soil water collected from 75 cm is centered around a global meteoric water line value of 10‰ (Fig.

682   8B). Based on data available from the National Weather Service (Chadron, NE), there were likely significant

683   precipitation events on 2022-06-25 and 2022-07-08 at the field site. There is a significant shift to lower $\delta^{18}O$ values

684   at a sampling depth of 25 cm between 2022-06-25 and 2022-06-29, as well as a marked increase in the d-excess

685   value (Fig. 8A). We interpret this shift as infiltration of precipitation with lower $\delta^{18}O$ values, and is supported by a

686   return of d-excess values to ~10‰ (Fig. 8A). The National Weather Service reported 0.84 inches of rain at Chadron

687   Municipal Airport, approximately 50 km from the study site on 2022-07-08, which likely was associated with at

688   least some precipitation at our field site. Following the significant rain event on 2022-07-08, we observe a marked

689   increase in the stable isotope value of water vapor from a sampling depth of 50 cm, towards values that are much

690   closer to those at 25 cm depth. This indicates that after a large precipitation event, there is mixing and the creation of

691   a far more uniform soil water isotope profile to a depth of 50 cm, but at the depth of 75 cm, the oxygen isotope data

692   remain fairly uniform across the sampling period.
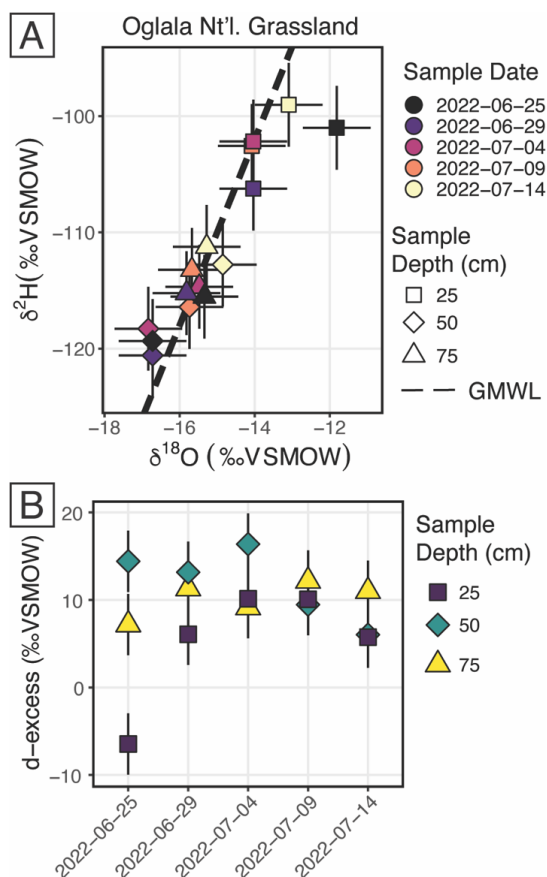
Figure 8. Results from the Oglala National Grassland, NE field site. A) δ^2H vs. $\delta^{18}O$, where the dashed line is the global meteoric water line. The shape of the depth sampled matches figure 7, and the color of the points is the date on which the soil water was sampled B) A plot of d-excess. Note, both the color and shape match figure 7.

717

718

719

720   At Briggsdale, CO we used the SWISS named Raclette to collect soil water vapor samples. Data from 25

721 cm depth at Briggsdale, CO were discarded because the water vapor mole fraction was much lower than would be

722 expected given the soil temperature (i.e. < 15,000 ppm). The gravimetric water concentration at that soil depth at the

723 time of sampling was approximately 4% through the sampling period. Given the low water concentration, it is

724 possible that there was simply not enough water vapor to sufficiently sample. Based on the results of the August

725 2022 water vapor test done on Raclette where all flasks fell within uncertainty of the SWISS system for both $\delta^{18}O$

726 and δ^2H, except for flask 11 (Figs. 4C and 5C), which corresponds to the 25 cm depth sample from 2022-07-27, we

727 interpret all of the data with a higher level of confidence. This sample was already removed from the dataset because

728 of low water vapor mole fraction associated with the very dry soil. The soil water $\delta^{18}O$ and δ^2H values from a

729 sampling depth of 50 cm and 75 cm overlap within uncertainty, but the soil water $\delta^{18}O$ and δ^2H values from 50 cm

730 have a higher isotopic value than the samples from 75 cm. All of the data from within each sampling depth group

731 (i.e. 50 cm and 75 cm) overlap within uncertainty, conforming to the expectation that soil water from these sampling

732 depths should be fairly invariant (e.g. Oerter et al., 2017). There were precipitation events at the study site on 2022-

733   07-24, 2022-07-28 and 2022-07-31. It is possible that the slight negative shift in both $\delta^{18}O$ and δ^2H on 2022-08-01

734   reflects infiltration of precipitation to those depths, but this is not certain given that all of the measurements from

735   within a sampling depth overlap within uncertainty.

736   At Seibert, CO we used the SWISS named Toblerone to collect soil water vapor samples. Data from 75 cm

737   depth at Seibert, CO were discarded because of evidence of condensation during the measurement of the flasks

738   associated with that sampling depth. Based on the results of the August 2022 water vapor test done on Toblerone,

739   we interpret all of the data with a high degree of confidence, except for Flask 3, which is the 50 cm sample from

740   2022-06-19 (Figs. 4C and 5C). Unlike data from the other two field sites, soil water from 25 cm and 50 cm overlap

741   within uncertainty. There were two precipitation events at the field site during the sampling period on 2022-06-25

742   and 2022-07-01, but both events were quite small (<0.02 inches, CoAgMet). There is no significant influence of the

743   precipitation events on the $\delta^{18}O$ and δ^2H values. The >1.0‰ increase in $\delta^{18}O$ values on 2022-06-29 is surprising

744   given that there is not a comparable magnitude increase in δ^2H value, and that the values measured from 2022-07-04

745   more closely match the $\delta^{18}O$ and δ^2H values from the two earlier sampling days. There are two potential

746   explanations for this data. First, that is a real signal from an evaporation driven increase in the $\delta^{18}O$ value, and the

747   reset to a lighter $\delta^{18}O$ value on 2022-07-04 is due to the infiltration of precipitation. This explanation is corroborated

748   by a low d-excess value associated with this measurement (Fig. SI 9). The second possible explanation is that the 25

749   cm sample from 2022-06-29 is influenced by condensation at the time of sampling. Dew point at the field site on

750   2022-06-29 significantly decreased as compared to the other sampling days to a monthly minimum of 20.6°C. It is

751   possible that environmental conditions encouraged the formation of condensation in the impermeable tubing at the

752   time of sampling. There were no obvious signs of condensation during the time of measurement in the lab. These

753   results highlight the utility of having broad contextual environmental data to aid in the interpretation of soil water

754   isotope data.

755   All together, these three soil water isotope datasets demonstrate two main findings. First, data from these

756   samples show that the differences between field sites is easily resolvable using the SWISS. For example, at 50 cm

757   depth the oxygen isotopes range between -14.4 to -16.3‰, -9.9 to -10.3‰, and -7.4 to -9.3‰ for the Oglala,

758   Briggsdale and Seibert sites, respectively. These differences likely reflect differences in the stable isotope

759   composition of precipitation and evaporation dynamics. Second, the sample data retrieved from a SWISS are

760   sufficiently precise to be able to meaningfully resolve vertical profile soil water isotope data. For example, at the

761   Oglala National Grassland field site, soil water from 25 cm clearly has higher $\delta^{18}O$ and δ^2H values as compared to

762   soil water from a depth of 50 and 75 cm.

763

764   **6. 3 Future improvements**

765   One significant SWISS unit hardware improvement that could be made would be to install a heating

766   implement to the flasks. One source of uncertainty on the current system is the potential effect of uneven heating of

767   the flasks prior to measurement. This could be improved in subsequent iterations of the SWISS with the addition of

768   heat tape or blankets that can deliver controlled and consistent amounts of heat. This improvement could also help

769   limit the amount of manual intervention needed during measurement, and could improve automation of flask

770   measurement.

771   In addition, we have made a few improvements to the automation system that were not implemented for the

772   data presented in this contribution, but will be part of future deployments. First, we will track conditions inside the

773   SWISS with a temperature and relative humidity sensor inside the case. Second, we plan to eliminate the power

774   inverter by powering both the Valco valve and mass flow controller with VDC using a power step up controller.

775   Lastly, we will add an IoT cellular router to be able to remotely monitor and control the SWISS units.

776   Finally, there are two future considerations for field deployments. The first is finding a way to safely and

777   automatically heat the impermeable tubing that connects the water vapor probes and the SWISS in a way that

778   doesn't change the inherent thermal structure of the soil, and is safe for unmonitored use. Additionally, we plan to

779   test SWISS unit resilience during air travel so that these units can be used at field sites that are not within driving

780   distance of a research facility.

781   **Conclusions**

782   We presented the evolution of the soil water isotope storage system (SWISS) from a prototype to a fully

783   built out and tested system. We also presented a quality control and quality assurance procedure that can be used to

784   ensure the reliable storage of soil water vapor over long time periods (up to 40 days). In addition, these quality

785   control and quality assurance tests shed light on the accuracy and precision of the SWISS. After applying an offset

786   correction, we determine the overall precision of the SWISS to be 0.9‰ and 3.7‰ for $\delta^{18}O$ and $\delta^{2}H$, respectively. In

787   a field setting, flasks reliably resist atmospheric intrusion. Additionally, the proposed sampling schema does not

788   introduce significant memory effects. Lastly, we demonstrate that the precision of the SWISS still allows us to

789   distinguish between field sites and between soil water dynamics within a single soil column. Taken as a whole, these

790   data show that the SWISS can be used as a tool to answer many emerging ecohydrological questions, and will

791   enhance researchers' ability to collect soil water isotope datasets from more remote and traditionally understudied

792   field sites.

793   **Acknowledgements**

794   We thank the numerous field assistants who helped to make the field work presented in this paper possible,

795   including Spencer Burns, Anne Fetrow, Sarah Brookins, Juliana Olsen-Valdez, and Haley Brumberger. We

796   acknowledge that both field work and laboratory work for this study was done on the traditional territories and

797   ancestral homelands of the Arapahoe, Ute and Cheyenne peoples. This work was supported by startup funding from

798   CU Boulder and NSF funding from grant EAR-2023385 awarded to K. Snell. Additionally, this work was supported

799   by the University of Colorado Boulder Beverly Sears Research Grant and the Clay Minerals Society Graduate

800   Student Research Grant both awarded to R. Havranek. CUBES–SIL is a CU Boulder Core Facility associated with

801   RRID: SCR_019300.

802

803 **Author contribution**

804 Rachel E. Havranek: original draft, conceptualization, methodology, investigation, formal analysis, funding

805 acquisition. Kathryn E. Snell: Conceptualization, Methodology, Writing – review & editing, funding acquisition.

806 Sebastian H. Kopf: Conceptualization, Methodology, Writing – review & editing. Brett Davidheiser-Kroll:

807 Conceptualization, Methodology, Writing – review & editing. Valerie Morris: Methodology, Writing – review &

808 editing. Bruce Vaugh: Methodology, Writing – review & editing.

809

810 **Competing interests**

811 The authors declare no competing interests.

Works Cited

Barnes, C. J., & Allison, G. B. (1983). The distribution of deuterium and 18O in dry soils. 1. Theory. *Journal of Hydrology*, *60*, 141–156.

Beyer, M., Kühnhammer, K., & Dubbert, M. (2020). In situ measurements of soil and plant water isotopes : a review of approaches , practical considerations and a vision for the future. *Hydrology and Earth System Sciences*, *24*, 4413–4440. https://doi.org/https://doi.org/10.5194/hess-24-4413-2020

Bowen, G. J., Cai, Z., Fiorella, R. P., & Putman, A. L. (2019). Isotopes in the Water Cycle: Regional- to Global-Scale Patterns and Applications. *Annual Review of Earth and Planetary Sciences*, *47*(1), 453–479. https://doi.org/10.1146/annurev-earth-053018-060220

Bowen, G. J., Putman, A., Brooks, J. R., Bowling, D. R., Oerter, E. J., & Good, S. P. (2018). Inferring the source of evaporated waters using stable H and O isotopes. *Oecologia*, *187*(4), 1025–1039. https://doi.org/10.1007/s00442-018-4192-5

Brooks, J. R., Barnard, H. R., Coulombe, R., & McDonnell, J. J. (2010). Ecohydrologic separation of water between trees and streams in a Mediterranean climate. *Nature Geoscience*, *3*(2), 100–104. https://doi.org/10.1038/ngeo722

Dawson, T. E., & Ehleringer, J. R. (1991). Streamside trees that do not use stream-water: evidence from hydrogen isotopes ratios. *Nature*, *350*(March), 335–337.

Gaj, M., Beyer, M., Koeniger, P., Wanke, H., Hamutoko, J., & Himmelsbach, T. (2015). In-situ unsaturated zone stable water isotope (2H and 18O) measurements in semi-arid environments using tunable off-axis integrated cavity output spectroscopy. *Hydrology and Earth System Sciences Discussions*, *12*(6), 6115–6149. https://doi.org/10.5194/hessd-12-6115-2015

Gómez-Navarro, C., Pataki, D. E., Bowen, G. J., & Oerter, E. J. (2019). Spatiotemporal variability in water sources of urban soils and trees in the semiarid, irrigated Salt Lake Valley. *Ecohydrology*, *12*(8). https://doi.org/10.1002/eco.2154

Good, S. P., Noone, D., & Bowen, G. J. (2015). Hydrologic connectivity constrains partitioning of global terrestrial water fluxes. *Science*, *349*(6244), 175–177. https://doi.org/10.1126/science.aaa5931

Havranek, R. E., Snell, K. E., Davidheiser-Kroll, B., Bowen, G. J., & Vaughn, B. (2020). The Soil Water Isotope Storage System (SWISS): An integrated soil water vapor sampling and multiport storage system for stable isotope geochemistry. *Rapid Communications in Mass Spectrometry*, *34*(12), 1–11. https://doi.org/10.1002/rcm.8783

842   Hinckley, E.-L. S., Barnes, R. T., Anderson, S. P., Williams, M. W., & Bernasconi, S. M. (2014). Nitrogen retention
843   and transport differ by hillslope aspect at the rain-snow transition of the Colorado Front Range. *Journal of*
844   *Geophysical Research: Biogeosciences*, *119*, 12811896. https://doi.org/10.1002/2013JG002588

845   Kübert, A., Paulus, S., Dahlmann, A., Werner, C., Rothfuss, Y., Orlkowski, N., & Dubbertm Maren. (2020). Water
846   Stable Isotopes in Ecohydrological Field Research : Comparison Between In Situ and Destructive Monitoring
847   Methods to Determine Soil Water Isotopic Signatures. *Frontiers in Plant Science*, *11*(April), 1–13.
848   https://doi.org/10.3389/fpls.2020.00387

849   Kühnhammer, K., Dahlmann, A., Iraheta, A., Gerchow, M., Birkel, C., Marshall, J. D., & Beyer, M. (2022).
850   Continuous in situ measurements of water stable isotopes in soils, tree trunk and root xylem: Field approval.
851   *Rapid Communications in Mass Spectrometry*, *36*(5). https://doi.org/10.1002/rcm.9232

852   Mahindawansha, A., Orlowski, N., Kraft, P., Rothfuss, Y., Racela, H., & Breuer, L. (2018). Quantification of plant
853   water uptake by water stable isotopes in rice paddy systems. *Plant and Soil*, *429*(1–2), 281–302.
854   https://doi.org/10.1007/s11104-018-3693-7

855   Oerter, E. J., Perelet, A., Pardyjak, E., & Bowen, G. J. (2016). Membrane inlet laser spectroscopy to measure H and
856   O stable isotope compositions of soil and sediment pore water with high sample throughput. *Rapid*
857   *Communications in Mass Spectrometry*, *31*(1), 75–84. https://doi.org/10.1002/rcm.7768

858   Oerter, E. J., & Bowen, G. J. (2017). In situ monitoring of H and O stable isotopes in soil water reveals
859   ecohydrologic dynamics in managed soil systems. *Ecohydrology*, *10*(4), 1–13.
860   https://doi.org/10.1002/eco.1841

861   Oerter, E. J., & Bowen, G. J. (2019). Spatio-temporal heterogeneity in soil water stable isotopic composition and its
862   ecohydrologic implications in semiarid ecosystems. *Hydrological Processes*, *March*, 1–15.
863   https://doi.org/10.1002/hyp.13434

864   Peterson, B. J., & Fry, B. (1987). Stable Isotopes in Ecosystem Studies. *Annual Reviews of Ecology and Systematics*,
865   *18*, 293–320. http://www.jstor.org/stable/2097134 REFERENC

866   Quade, M., Klosterhalfen, A., Graf, A., Brüggemann, N., Hermes, N., Vereecken, H., & Rothfuss, Y. (2019). In-situ
867   monitoring of soil water isotopic composition for partitioning of evapotranspiration during one growing season
868   of sugar beet (Beta vulgaris). *Agricultural and Forest Meteorology*, *266–267*(December 2018), 53–64.
869   https://doi.org/10.1016/j.agrformet.2018.12.002

870   Quade, M., Brüggemann, N., Graf, A., Vanderborght, J., Vereecken, H., & Rothfuss, Y. (2018). Investigation of
871   Kinetic Isotopic Fractionation of Water during Bare Soil Evaporation. *Water Resources Research*, *54*(9),
872   6909–6928. https://doi.org/10.1029/2018WR023159

873 Rothfuss, Y., Vereecken, H., & Brüggemann, N. (2013). Monitoring water stable isotopic composition in soils using
874   gas-permeable tubing and infrared laser absorption spectroscopy. *Water Resources Research*.
875   https://doi.org/10.1002/wrcr.20311

876 Rothfuss, Y., Merz, S., Vanderborght, J., Hermes, N., Weuthen, A., Pohlmeier, A., Vereecken, H., & Brüggemann,
877   N. (2015). Long-term and high-frequency non-destructive monitoring of water stable isotope profiles in an
878   evaporating soil column. *Hydrology and Earth System Sciences*, *19*(10), 4067–4080.
879   https://doi.org/10.5194/hess-19-4067-2015

880 Rothfuss, Y., Quade, M., Brüggemann, N., Graf, A., Vereecken, H., & Dubbert, M. (2021). Reviews and syntheses:
881   Gaining insights into evapotranspiration partitioning with novel isotopic monitoring methods. In
882   *Biogeosciences* (Vol. 18, Issue 12, pp. 3701–3732). Copernicus GmbH. https://doi.org/10.5194/bg-18-3701-
883   2021

884 Soderberg, K., Good, S. P., Wang, L., & Caylor, K. (2012). Stable Isotopes of Water Vapor in the Vadose Zone: A
885   Review of Measurement and Modeling Techniques. *Vadose Zone Journal*, *11*(3), 0.
886   https://doi.org/10.2136/vzj2011.0165

887 Soil Survey Staff, Natural Resources Conservation Service, United States Department of Agriculture. Soil Series
888   Classification Database. Available online. Accessed 09/10/2022.

889 Sprenger, M., Leistert, H., Gimbei, G., & Weiler, M. (2016). Illuminating hydrological processes at the soil-
890   vegetation-atmosphere interface with water stable isotopes. *Reviews in Geophysics*, *54*, 674–704.
891   https://doi.org/10.1002/ 2015RG000515

892 Sprenger, M., & Allen, S. T. (2020). What Ecohydrologic Separation Is and Where We Can Go With It. In *Water*
893   *Resources Research* (Vol. 56, Issue 7). Blackwell Publishing Ltd. https://doi.org/10.1029/2020WR027238

894 Theis, D. E., Saurer, M., Blum, H., Frossard, E., & Siegwolf, R. T. W. (2004). A portable automated system for
895   trace gas sampling in the field and stable isotope analysis in the laboratory. *Rapid Communications in Mass*
896   *Spectrometry*, *18*(18), 2106–2112. https://doi.org/10.1002/rcm.1596

897 Vereecken, H., Amelung, W., Bauke, S. L., Bogena, H., Brüggemann, N., Montzka, C., Vanderborght, J., Bechtold,
898   M., Blöschl, G., Carminati, A., Javaux, M., Konings, A. G., Kusche, J., Neuweiler, I., Or, D., Steele-Dunne, S.,
899   Verhoef, A., Young, M., & Zhang, Y. (2022). Soil hydrology in the Earth system. *Nature Reviews Earth &*
900   *Environment*. https://doi.org/10.1038/s43017-022-00324-6

901 Volkmann, T. H. M., & Weiler, M. (2014). Continual in situ monitoring of pore water stable isotopes in the
902   subsurface. *Hydrology and Earth System Sciences*, *18*(5), 1819–1833. https://doi.org/10.5194/hess-18-1819-
903   2014

904   Zimmermann, U., Munnich, K. O., & Roether, W. (1966). Tracers Determine Movement of Soil Moisture and

905   Evapotranspiration. *Science*, *152*(3720), 346–347. https://doi.org/10.1126/science.152.3720.346

906